MATERIALS SCIENCE

Acceptor plane expansion enhances horizontal orientation of thermally activated delayed fluorescence emitters

Yepeng Xiang[1,2], Pan Li[3], Shaolong Gong[1]*, Yu-Hsin Huang[3], Chun-Yu Wang[3], Cheng Zhong[1], Weixuan Zeng[1], Zhanxiang Chen[1], Wei-Kai Lee[3], Xiaojun Yin[2], Chung-Chih Wu[3]*, Chuluo Yang[1,2]*

Manipulating orientation of organic emitters remains a formidable challenge in organic light-emitting diodes (OLEDs). Here, expansion of the acceptor plane of thermally activated delayed fluorescence (TADF) emitters was demonstrated to selectively modulate emitting dipole orientation. Two proof-of-the-concept molecules, PXZPyPM and PXZTAZPM, were prepared by introducing a planar 2-phenylpyridine or 2,4,6-triphenyl-1,3,5-triazine substituent into a prototypical molecule (PXZPM) bearing a pyrimidine core and two phenoxazine donors. This design approach suppressed the influence of substituents on electronic structures and associated optoelectronic properties. Accordingly, PXZPyPM and PXZTAZPM preserved almost the same excited states and similar emission characteristics as PXZPM. The expanded acceptor plane of PXZPyPM and PXZTAZPM resulted in a 15 to 18% increase in horizontal ratios of emitting dipole orientation. PXZPyPM supported its green device exhibiting an external quantum efficiency of 33.9% and a power efficiency of 118.9 lumen per watt, competitive with the most efficient green TADF OLEDs reported so far.

INTRODUCTION

In the field of organic light-emitting diodes (OLEDs), molecular electronic structure and molecular orientation are two key factors that strongly determine optoelectronic properties of organic semiconductor amorphous films such as emission, absorption, energy level, and charge carrier mobility (*1*–*4*). To date, various methods have been reported to actively control electronic structure and the associated key optoelectronic properties. To illustrate, heavy metal–based phosphorescent emitters and thermally activated delayed fluorescence (TADF) emitters have been demonstrated by actively modulating the electronic structure of the emitters (*5*–*8*). For the latter factor, a handful of strategies have been reported to be capable of controlling molecular orientation (*1*, *9*–*21*). For example, Kido and co-workers (*12*) recently reported a series of electron-transporting materials with horizontal molecular orientation induced by intermolecular weak hydrogen bonds.

Controlling the molecular orientation of organic emitters to improve their horizontal ratios of emitting dipole orientation ($\Theta_{//}$) has recently attracted considerable attention because this holds great promise in improving optical out-coupling efficiency (η_{out}) and the corresponding external quantum efficiency (EQE) of OLEDs (*13*–*21*). Using phosphorescent and TADF emitters with 100% $\Theta_{//}$ can boost the theoretical limit of η_{out} and EQE to ~45% in conventional planar OLED structure without the introduction of extra light extraction technologies (*9*, *21*). So far, considerable progress has been made on phosphorescent emitters with preferentially horizontal emitting dipole orientation, and the corresponding devices have achieved more than 30% EQEs for full-color phosphorescent OLEDs. However, the requirement for coordination geometry of heavy metal phosphors limits regulation freedom of molecular orientation and the related emitting dipole orientation (*22*, *23*). Comparatively, TADF emitters provide a more flexible platform to control molecular orientation and the associated emitting dipole orientation, owing to their large structure diversity arising from numerous donor/acceptor combination and various linking space/topology (*3*, *8*). Similar to conventional fluorescent emitters and heavy metal phosphors, elongating the molecular length and enlarging the molecular planarity are highly desirable to construct TADF emitters with preferentially horizontal emitting dipole orientation (*13*–*20*). Among these two methods, elongating the molecular length seems to be more preferable to develop TADF emitters with high $\Theta_{//}$ because it matches well with design requirement of D-A or D-π-A architecture for TADF molecules. Following this concept, some state-of-the-art blue, green, and orange-red TADF emitters with high $\Theta_{//}$ have been developed, and their OLEDs have demonstrated record-high device performance with close to or more than 30% EQE (*13*–*16*). For instance, we recently reported that a spiroacridine-triazine TADF molecule yielded a high $\Theta_{//}$ of 83% and supported its sky-blue TADF OLED with nearly 37% EQE (*14*). On the other hand, some TADF emitters with high $\Theta_{//}$ have also been reported by enlarging the molecular planarity (*17*–*19*). However, modulating molecular orientation and the associated emitting dipole orientation of TADF emitters typically leads to simultaneous change of electronic structure of TADF emitters (*14*–*17*, *19*). This, in turn, results in notable influence on excited states, energy levels, and emission characteristics of TADF emitters. Thus, selectively modulating molecular orientation and the related emitting dipole orientation of TADF emitters remains as one of the most significant issues for the development of ultrahigh-efficiency TADF OLEDs.

To address this issue, we recently studied the correlation between molecular structure and transition dipole moment (TDM)

[1]Department of Chemistry, Hubei Key Lab on Organic and Polymeric Optoelectronic Materials, Wuhan University, Wuhan 430072, P. R. China. [2]Shenzhen Key Laboratory of Polymer Science and Technology, College of Materials Science and Engineering, Shenzhen University, Shenzhen 518060, P. R. China. [3]Department of Electrical Engineering, Graduate Institute of Electronics Engineering and Graduate Institute of Photonics and Optoelectronics, National Taiwan University, Taipei 10617, Taiwan.
*Corresponding author. Email: slgong@whu.edu.cn (S.G.); wucc@ntu.edu.tw (C.-C.W.); clyang@szu.edu.cn (C.Y.)

direction of TADF emitters using the nuclear ensemble approach (*24*). This method indicates that delicate molecular design may reveal the potential in selectively controlling emitting dipole orientation of TADF emitters. Following this revelation, we thereby proposed an acceptor plane expansion approach in the molecular design of TADF emitters with the goals of selectively modulating their molecular orientation and the associated alignment of emitting dipole orientation. To validate our concept, we designed and synthesized two star-shaped green TADF emitters, 10,10′-((2-(4-(pyridin-2-yl)phenyl)pyrimidine-4,6-diyl)bis(4,1-phenylene))bis(10*H*-phenoxazine) (PXZPyPM) and 10,10′-((2-(4-(4,6-diphenyl-1,3,5-triazin-2-yl)phenyl)pyrimidine-4,6-diyl)bis(4,1-phenylene))bis(10*H*-phenoxazine) (PXZTAZPM) (Fig. 1A), by incorporating two planar functional units, 2-phenylpyridine unit and 2,4,6-triphenyl-1,3,5-triazine unit, into electron acceptor pyrimidine moiety of a reference TADF emitter, PXZPM, with the aim to expand acceptor plane. PXZPM was selected for its boomerang molecular shape, high photoluminescence quantum efficiency (Φ_{PL}), distinct TADF nature, and feasible modification of molecular structure (*25*, *26*). With this approach, we selectively strengthened horizontal orientation of TADF emitters with negligible influence on the electronic structure. As a result, PXZPyPM and PXZTAZPM exhibited higher $\Theta_{//}$ than PXZPM while preserving almost the same highest occupied molecular orbital (HOMO)/lowest unoccupied molecular orbital (LUMO) energy levels and excited states, as well as similar emission characteristics as PXZPM. In comparison with the PXZPM-based reference device, using PXZPyPM and PXZTAZPM resulted in higher η_{out} of ~39% and significantly enhanced electroluminescence efficiencies with up to nearly 34% EQE and exceeding 118 lumen per watt (lm W^{-1}) power efficiency (PE). These performance metrics are comparable with the best results reported so far for green-to-yellow TADF OLEDs (*15*, *20*, *27*, *28*).

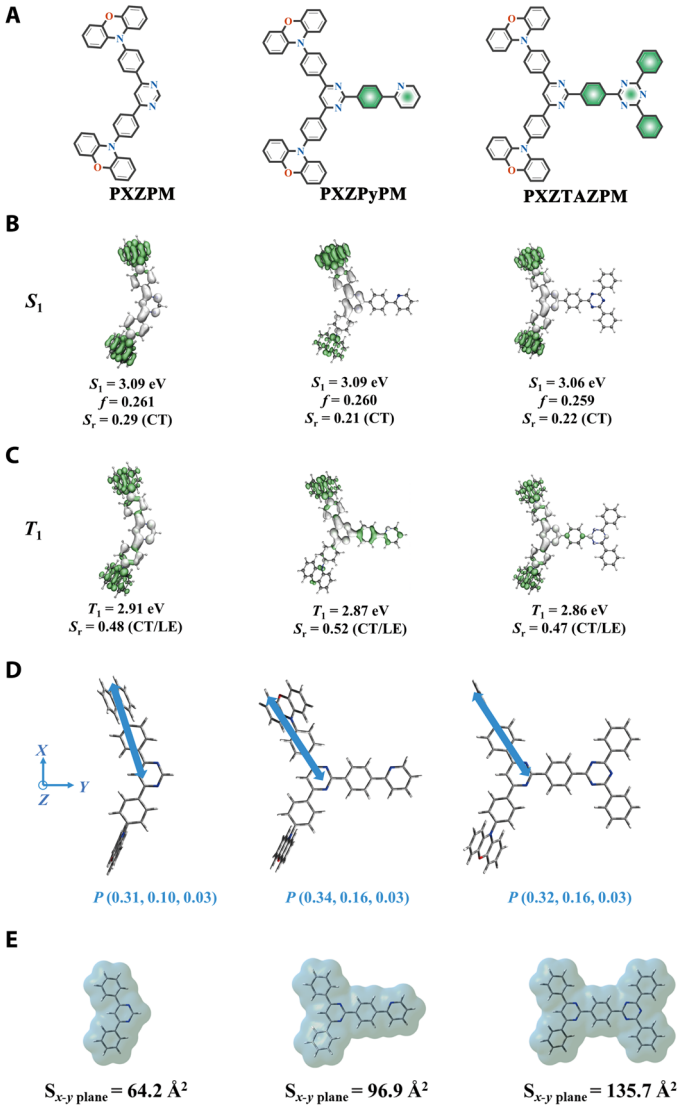

Fig. 1. Chemical structures and theoretical calculations of PXZPM, PXZPyPM, and PXZTAZPM. (**A**) Compounds studied in this work. (**B**) Calculated S_1 and (**C**) T_1 hole (green)–electron (light gray) distributions, energy levels, oscillator strengths (*f*), and *Sr* indexes with the optimized structures of excited states of PXZPM, PXZPyPM, and PXZTAZPM. CT, charge transfer; LE, locally excited. (**D**) The direction of the calculated TDM (as indicated by arrow) relative to the coordinate of the molecular structure. (**E**) The area of the corresponding acceptor moiety (*x*-*y* plane).

RESULTS

To explore the influence of different substituent groups on the frontier molecular orbital and electronic structure of PXZPyPM and PXZTAZPM, density functional theory (DFT) and time-dependent DFT (TD-DFT) were performed on both molecules (*29*, *30*). We also performed the same theoretical simulation on the prototypical molecule of PXZPM to be used for comparison (fig. S3). The frontier molecular orbital analysis revealed that the HOMOs of PXZPyPM and PXZTAZPM were mainly located on the phenoxazine unit with small distributions on the adjacent phenylene bridges, the same as PXZPM. Accordingly, three molecules had almost the same HOMO levels of about −4.7 eV. These results indicated that the introduction of 2-phenylpyridine or 2,4,6-triphenyl-1,3,5-triazine unit in the pyrimidine acceptor has a negligible effect on the HOMO distributions and the corresponding energy levels. In comparison with PXZPM, PXZPyPM exhibited the same LUMO distributions, mainly localizing on the pyrimidine unit and the adjacent phenylene bridges. Notably, the LUMO of PXZTAZPM was mostly distributed on the pyrimidine unit and the 2,4,6-triphenyl-1,3,5-triazine group, mainly due to the stronger acceptor strength of the 2,4,6-triphenyl-1,3,5-triazine unit with respect to the 4,6-diphenylpyrimidine group (the LUMO level of 2,4,6-triphenyl-1,3,5-triazine is lower than that of the 4,6-diphenylpyrimidine, as shown in fig. S3A). Despite different LUMO distributions, both PXZPyPM and PXZTAZPM had well-separated frontier molecular orbital distributions, accompanied by small frontier molecular orbital overlap. This results in small energy gaps (ΔE_{ST}s) between the lowest triplet excited state (T_1) and the lowest singlet excited state (S_1) for PXZPyPM and PXZTAZPM, similar to PXZPM. Such small ΔE_{ST}s could benefit the reverse intersystem crossing (RISC) process from T_1 to S_1 for PXZPyPM and PXZTAZPM with the thermal aid from the surroundings (*4*, *31*). Furthermore, the excited state analysis (Fig. 1, B and C, and table S1) revealed that S_1 states of PXZPyPM and PXZTAZPM were dominant by the charge transfer transitions between the phenoxazine and 4,6-diphenylpyrimidine moieties, similar to PXZPM. Meanwhile, the holes/electrons of S_1 states for three molecules were mainly distributed on the phenoxazine and 4,6-diphenylpyrimidine units, respectively (*32*). Consequently,

PXZPyPM and PXZTAZPM had almost the same S_1 energy levels as PXZPM. On the other hand, the T_1 states of three molecules exhibited charge transfer/locally excited hybrid character, coupled with similar values. In addition, three molecules had similar oscillator strengths (*f*s), suggesting similar $S_1 \rightarrow S_0$ radiative rates for these molecules (*33*). These results strongly indicated that the introduction of 2-phenylpyridine unit or 2,4,6-triphenyl-1,3,5-triazine unit in the pyrimidine acceptor has a small influence on their electronic structures and the related energy levels and excited states.

On the other hand, the optimized molecular structures of PXZPM, PXZPyPM, and PXZTAZPM (Fig. 1D) revealed that, although the phenoxazine groups preferred highly twisted configuration at their nitrogen positions, all molecules mainly located in their corresponding *x*-*y* plane, resulted in predominantly planar structures originating from the expanded acceptor plane. This was further verified by x-ray crystallographic analysis. The single-crystal structure of the PXZPyPM compound was dominated by the large planarity acceptor plane (fig. S4A), which is basically coincident with the DFT-optimized structure (fig. S4B) (*34*). Moreover, PXZPyPM molecules preferred nearly parallel alignment to its acceptor plane in the crystal packing diagram. All these properties may benefit horizontal emitting dipole orientation of PXZPyPM and PXZTAZPM. To determine this point, we first simulated $S_1 \rightarrow S_0$ TDMs for PXZPM, PXZPyPM, and PXZTAZPM using the nuclear ensemble approach (*24*). Similar to PXZPM (Fig. 1D), the TDM vectors coordinates of PXZPyPM and PXZTAZPM were (0.34, 0.16, 0.03) and (0.32, 0.16, 0.03). These parameters indicated that all TDM vectors of three molecules mainly aligned on the plane of their corresponding acceptor moieties (*x*-*y* plane). This may make their TDM horizontally aligned when anchored onto a substrate surface. In this sense, one could enhance horizontal TDM via increasing planarity of acceptor plane. To reveal the influence of different substituent moieties on planarity of acceptor moieties, we quantified areas of the corresponding acceptor plane of three molecules using the isodensity surface by Marching Tetrahedra approach (*35*). As expected (Fig. 1E), the areas of acceptor plane for three molecules exhibited the sequence of 64.2 $Å^2$ (PXZPM) < 96.9 $Å^2$ (PXZPyPM) < 135.7 $Å^2$ (PXZTAZPM). This may possibly result in gradually enhanced horizontal emitting dipole orientation for the corresponding emitters.

For practical applications in OLEDs, emitter molecules are generally doped into some suitable host matrixes to form amorphous emitting layers via a vacuum deposition process. In such host-guest systems, molecular orientation and the associated emitting dipole orientations of emitters can be affected by many factors, such as the emitter, the host, and the substrate as well as the complicated interactions among them (*11*, *17*). Meanwhile, the amorphous nature of the doped emitting layers inhibits experimental observation of molecular packing details of the emitters in the host matrix. To quantitatively evaluate the influence of acceptor plane on molecular orientation and the associated emitting dipole orientation of emitters in the emitting layer, we mimicked the vacuum deposition process of three emitters doped into the same 9-(3-(9*H*-carbazol-9-yl) phenyl)-9*H*-carbazole-3-carbonitrile (mCPCN) host via atomistic molecular dynamics simulations combined with quantum mechanical analyses, by following the similar methodology recently reported by Yi and co-workers (*36*, *37*). mCPCN is a widely used host material for TADF emitters, in virtue of its bipolar charge-transporting ability and a high triplet energy of ~3.0 eV (*38*). Figure 2A showed the final snapshots of the equilibrated emitting layer film with three emitters as the guest and mCPCN as the host. The atomistic molecular dynamics simulations results revealed that, although the host molecules exhibited relatively random orientation in the simulated emitting layers, emitter molecules preferred more horizontal molecular orientation when enlarging the acceptor plane of emitters. Owing to the good consistency between the TDM direction and the acceptor plane of these emitters, the TDMs of three emitters exhibited the same tendency with the average values of θ following the order of 60.8° (PXZPM) < 65.2° (PXZPyPM) < 66.4° (PXZTAZPM) (Fig. 2B), where the θ denoted the angle between the TDM of emitter molecule and the normal direction of the substrate surface. Accordingly, the theoretical $\Theta_{//}$ values calculated with $\langle \sin^2\theta \rangle$ were 76% for PXZPM, 82% for PXZPyPM, and 84% for PXZTAZPM (*1*). This strongly suggested that the larger acceptor plane of emitters can result in more parallel molecular orientation and horizontal emitting dipole orientation of emitters to the substrate when doping into the host matrix. To further confirm this point, we studied the emitting dipole orientation of three emitters in the same mCPCN host by performing the angle-dependent *p*-polarization–resolved photoluminescence intensity measurement. As shown in Fig. 2C, the experimental $\Theta_{//}$s of PXZPyPM and PXZTAZPM were estimated to be 84 and 86%, respectively. These values are significantly higher than the prototypical molecule PXZPM (73%) doped into the same host matrix with the same doping concentration [6.0 weight % (wt %)]. The experimental $\Theta_{//}$ tendency is in good agreement with the atomistic molecular dynamics simulation results. Furthermore, the extracted $\Theta_{//}$s of three emitters remained almost the same upon different doping concentrations in the mCPCN host (fig. S5, A to C). In addition, we also studied the angle-dependent *p*-polarized emission intensities of PXZPM, PXZPyPM, and PXZTAZPM in the widely used host material of CBP [4,4′-di(9*H*-carbazol-9-yl)-1,1′-biphenyl] (fig. S5D). The extracted $\Theta_{//}$s of three emitters were 69% for PXZPM, 79% for PXZPyPM, and 81% for PXZTAZPM in the CBP host. The $\Theta_{//}$ tendency of three emitters in the CBP host is basically consistent with the $\Theta_{//}$ order of these emitters in the mCPCN host. These results strongly established the horizontal emitting dipole orientations as the intrinsic nature of PXZPyPM and PXZTAZPM. Combining the theoretical simulation and experimental data, we can conclude that the acceptor expansion approach can actively enhance horizontal molecular orientation and thus strengthen horizontal emitting dipole orientation of emitters. This may benefit the optical out-coupling efficiencies of their OLEDs.

PXZPyPM and PXZTAZPM exhibited high decomposition temperatures (corresponding to 5% weight loss) of over 480°C, together with high glass transition temperatures of 162°C for PXZPyPM and 185°C for PXZTAZPM (fig. S6, A and B). These values are higher than that of PXZPM (the decomposition temperature of 488°C and the glass transition temperature of 115°C) (*25*), mainly due to the increased molecular weight (table S2). We studied the electrochemical properties of both emitters by cyclic voltammetry experiments. PXZPyPM and PXZTAZPM exhibited reversible oxidation behaviors belonging to the phenoxazine donor (fig. S6C). Providing the optical band gaps of both emitters, the HOMO/LUMO levels were −5.08/−2.36 eV for PXZPyPM and −5.10/−2.44 eV for PXZTAZPM, similar to the HOMO/LUMO level of −5.10/−2.42 eV for PXZPM. These results suggest that the introduction of 2-phenylpyridine or 2,4,6-triphenyl-1,3,5-triazine unit in the pyrimidine acceptor has a small impact on the HOMO/LUMO levels. Meanwhile, the obtained

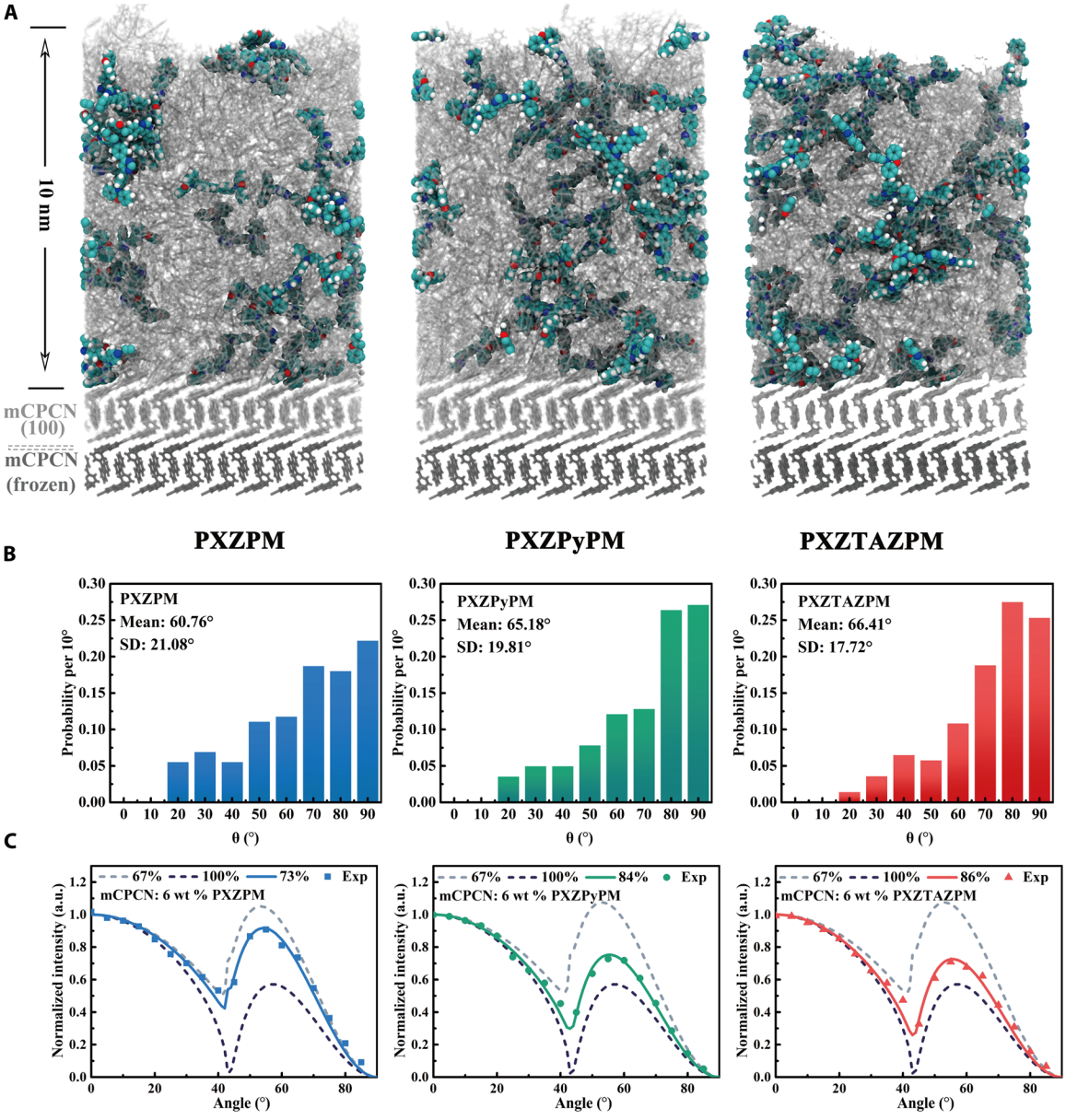

Fig. 2. Atomistic molecular dynamics simulations and *p*-polarized measurements for PXZPM, PXZPyPM, and PXZTAZPM. (**A**) Snapshots of the final deposition for PXZPM, PXZPyPM, and PXZTAZPM molecules doped into mCPCN host molecules on the mCPCN (100) substrate surfaces. (**B**) The probability per 10° distribution of TDMs for PXZPM, PXZPyPM, and PXZTAZPM by atomistic molecular dynamics simulations. (**C**) Measured (symbols) *p*-polarized photoluminescence intensity (at photoluminescence peak wavelength) of different emitting layers as a function of the emission angle and simulated curves (lines and dashed lines) with different horizontal dipole ratios ($\Theta_{//}$s) of PXZPM, PXZPyPM, and PXZTAZPM doped into the mCPCN host (6.0 wt %). a.u., arbitrary units.

HOMO/LUMO levels were coincident with the DFT results (fig. S3 and table S2).

Absorption spectra of both emitters, PXZPyPM and PXZTAZPM, in toluene (Fig. 3A) exhibited similar absorption profiles as the prototypical compound PXZPM, composed of two types of absorption bands: strong, high-energy bands (280 to 355 nm), mainly corresponding to π-π* transitions of phenoxazine and/or the corresponding substituted pyrimidine moieties; and weak, low-energy bands in the region of 360 to 450 nm, assigned to intramolecular charge transfer transition from phenoxazine units to the corresponding acceptor units (*26*). Furthermore, both emitters in toluene solution displayed broad and structureless emission profiles with main peaks at 530 and 534 nm for PXZPyPM and PXZTAZPM, respectively, at 300 K. Similar to PXZPM, PXZPyPM and PXZTAZPM exhibited an obvious positive solvatochromic effect together with the red-shifted photoluminescence emission peaks from low polarity solvent of toluene to high polarity solvent of chloroform (fig. S7), which manifests their intramolecular charge transfer nature. Under the degassed condition, the transient photoluminescence decay curves of PXZPyPM and PXZTAZPM in toluene exhibited double-exponential decays containing prompt and delayed fluorescence components (Fig. 3B). The presence of oxygen, however, completely

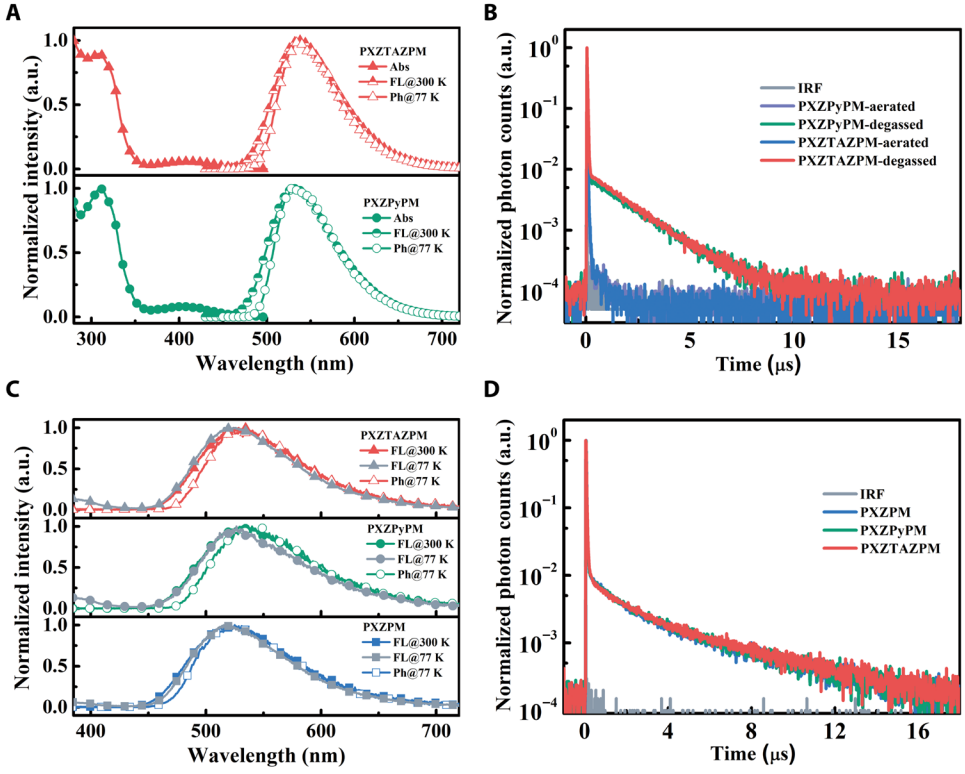

Fig. 3. Photoluminescence properties of PXZPM, PXZPyPM, and PXZTAZPM. (**A**) Normalized Ultraviolet-visible absorption and fluorescence spectra of PXZPyPM and PXZTAZPM in toluene (10^{-5} M) at 300 K and normalized phosphorescence (77 K) spectra of PXZPyPM and PXZTAZPM in 2Me-THF (10^{-5} M) (excitation wavelength, 365 nm). Abs, absorption; FL, fluorescence; Ph, phosphorescence. (**B**) Transient photoluminescence decay curves of PXZPyPM and PXZTAZPM in toluene (10^{-5} M) under aerated and degassed conditions, following excitation at 377 nm, detected at 530 and 534 nm (photoluminescence peak wavelength), respectively. The instrument response function (IRF) was also shown. (**C**) Normalized fluorescence (300 K), fluorescence (77 K), and phosphorescence (77 K) spectra of 6.0 wt % PXZPM, PXZPyPM, and PXZTAZPM doped into the mCPCN host (excitation wavelength, 365 nm). (**D**) Transient photoluminescence decay curves of 6.0 wt % PXZPM, PXZPyPM, and PXZTAZPM doped into the mCPCN host at 300 K, following excitation at 377 nm, detected at 521, 524, and 528 nm (photoluminescence peak wavelength), respectively. The IRF was also shown.

quenched the delayed fluorescence components of both emitters, resulting in single-exponential decays of only nanosecond-scale prompt fluorescence. This phenomenon suggested that both PXZPyPM and PXZTAZPM were effective triplet-harvesting emitters, similar to PXZPM (*25*). To emulate conditions relevant to OLED applications, the emission characteristics of PXZPyPM and PXZTAZPM in the mCPCN host were investigated. Both emitters in the mCPCN (6.0 wt %) host displayed intramolecular charge transfer–featured emission profiles peaking at 524 nm for PXZPyPM and 528 nm for PXZTAZPM (Fig. 3C and Table 1), slightly red-shifted to that of PXZPM (521 nm). Meanwhile, three emitters in the mCPCN host all had small ΔE_{ST}s of below 0.1 eV, which is favorable for effective RISC process from T_1 to S_1. The transient PL characterization of PXZPyPM and PXZTAZPM in the mCPCN host yielded similar biexponential decays comprising prompt and delayed fluorescence components with the corresponding lifetimes of 19.4 ns/2.77 μs for PXZPyPM and 20.4 ns/2.79 μs for PXZTAZPM at 300 K (Fig. 3D), close to PXZPM (20.2 ns/2.56 μs). Furthermore, the photoluminescence spectra of the delayed fluorescence for PXZPyPM and PXZTAZPM are basically identical to their corresponding photoluminescence spectra of the prompt fluorescence (fig. S8, D to F), and the delayed fluorescence components of PXZPyPM and PXZTAZPM were gradually increased from 100 to 300 K (fig. S8, G and H). These results clearly established distinct TADF nature of both emitters. At 300 K, PXZPyPM and PXZTAZPM in the mCPCN host had near-unity Φ_{PL}, the same as PXZPM. Moreover, three emitters had similar radiative rate constants ($k_r = 2.99 \times 10^7$ s^{-1} to 3.35×10^7 s^{-1}), comparable with efficient conventional fluorescent emitters ($k_r = 10^7$ to 10^8 s^{-1}) (*33*). Besides, the rate constants of ISC (k_{ISC}) and RISC (k_{RISC}) processes for PXZPyPM and PXZTAZPM in the mCPCN host were estimated to be 1.80×10^7 s^{-1}/5.57×10^5 s^{-1} for PXZPyPM and 1.69×10^7 s^{-1}/5.45×10^5 s^{-1} for PXZTAZPM, respectively, close to those of PXZPM (1.73×10^7 s^{-1}/6.02×10^5 s^{-1}) (*27*). To get more insights, we also studied the photophysical properties of three emitters in the polymethyl methacrylate (PMMA) films (fig. S9). Apparently, three emitters in the PMMA films (6.0 wt %) displayed similar emission profiles peaking at 516 nm for PXZPM, 518 nm for PXZPyPM, and 517 nm for PXZTAZPM. Furthermore, PXZPyPM and PXZTAZPM in the PMMA films had almost the same prompt and delayed fluorescence lifetimes of 19.9 ns/2.41 μs and 19.7 ns/2.43 μs, respectively, similar to that of PXZPM (23.3 ns/2.98 μs). PXZPyPM and PXZTAZPM in the PMMA films also exhibited the identical photoluminescence spectra in the prompt and delayed fluorescence, further verifying the TADF nature of both emitters.

Note that the acceptor plane expansion approach via introducing suitable substitution units with similar acceptor strength had a negligible effect on electronic structures and associated optoelectronic properties of PXZPyPM and PXZTAZPM compared with

Table 1. Photophysical properties of PXZPM, PXZPyPM, and PXZTAZPM.

Compound	PL_{max}* (nm)	S_1† (eV)	$S_{1,77K}$† (eV)	T_1† (eV)	ΔE_{ST}‡ (eV)	τ_p§ (ns)	τ_d§ (μs)	Φ_{PL}‖ (%)	Φ_p/Φ_d¶ (%)	k_r# (10^7 s^{-1})	k_{ISC}# (10^7 s^{-1})	k_{RISC}# (10^5 s^{-1})
PXZPM	521	2.62	2.58	2.54	0.04	20.2	2.56	100	65/35	3.22	1.73	6.02
PXZPyPM	524	2.60	2.60	2.53	0.07	19.4	2.77	100	65/35	3.35	1.80	5.57
PXZTAZPM	528	2.56	2.58	2.53	0.05	20.4	2.79	93	61/32	2.99	1.69	5.45

*Measured in the mCPCN host (6.0 wt %) at 300 K. †Calculated from the onset wavelengths of fluorescence (300 K), fluorescence (77 K), and phosphorescence (77 K) spectra of three emitters in the mCPCN host. ‡Calculated from the onset wavelengths of fluorescence (77 K) and phosphorescence (77 K) spectra of three emitters in the mCPCN host. §Measured in the mCPCN host (6.0 wt %) at 300 K. ‖Measured in the mCPCN host (6.0 wt %) under degassed condition at 300 K. The error for Φ_{PL} is ±1%. ¶The prompt and delayed fluorescence photoluminescence quantum efficiency under degassed condition at 300 K. #The radiative rate constant, rate constants of ISC, and RISC process of 6.0 wt % PXZPM, PXZPyPM, and PXZTAZPM doped into the mCPCN host at 300 K.

the prototypical emitter of PXZPM. Therefore, in comparison with PXZPM, PXZPyPM and PXZTAZPM not only had almost the same HOMO/LUMO energy levels and excited states but also retained similar emission characteristics including photoluminescence emission profiles, TADF nature, Φ_{PL}, k_r, k_{ISC}, and k_{RISC}. The expanded acceptor planes resulted in higher horizontal ratios of emitting dipole orientation for PXZPyPM and PXZTAZPM relative to PXZPM. In this sense, we have selectively strengthened horizontal ratios of emitting dipole orientation of PXZPyPM and PXZTAZPM with small influences on their electronic structures and related optoelectronic properties.

To explore the influence of selective modulation of emitting dipole orientation on electroluminescence performance, multilayer OLEDs using PXZPyPM and PXZTAZPM as the dopants were fabricated, following the typical configuration outlined in Fig. 4 (A and B). It consisted of indium tin oxide (ITO)/MoO_3 (1 nm)/1,1-bis[(di-4-tolylamino)phenyl]-cyclohexane (60 nm)/*N*,*N*-dicarbazolyl-3,5-benzene (10 nm)/emitting layer (20 nm)/tris-[3-(3-pyridyl)mesityl] borane (55 nm)/LiF (1 nm)/Al (Fig. 4A). The reference device A was based on the prototypical emitter of PXZPM. On the other hand, on the basis of the same device architecture as device A, PXZPyPM and PXZTAZPM were doped into the mCPCN host with an optimal doping concentration of 6.0 wt % to serve as the emitting layers for devices B and C, respectively (fig. S10 and table S3).

As shown in Fig. 4C, devices A to C exhibited similar current density–voltage (*J*-*V*) characteristics and the same turn-on voltages (V_{on}, recorded at a luminance of 1 cd m^{-2}) of 3.0 V (Table 2). This can be attributed to the same device architecture and the similar HOMO/LUMO levels of three emitters (table S2). Devices A to C displayed the same electroluminescence profiles peaking at 528 nm (Fig. 4D), corresponding to the same Commission International de l'Eclairage 1931 (CIE 1931) coordinates of (0.33, 0.58) for devices A to C. The PXZTAZPM-based device C exhibited a maximum current efficiency (CE_{max}) of 101.3 cd A^{-1}, a maximum PE (PE_{max}) of 106.1 lm W^{-1}, and a maximum EQE (EQE_{max}) of 30.1%. Comparatively, the higher Φ_{PL} and similar $\Theta_{//}$ of PXZPyPM endowed device B with a better electroluminescence (EL) performance with a CE_{max} of 113.5 cd A^{-1}, a PE_{max} of 118.9 lm W^{-1}, and an EQE_{max} of 33.9% without introducing any extra light extraction technology (Fig. 4E). To the best of our knowledge, these efficiencies of device B are among the highest EL performance for green-to-yellow TADF OLEDs (table S4) (*15*, *20*, *27*, *28*). As a whole, the EL efficiencies of devices B and C both outperformed the PXZPM-based reference device A (98.4 cd A^{-1}, 103.5 lm W^{-1}, and 29.5%). On account of similar photophysical properties (TADF nature, Φ_{PL}, k_r, k_{ISC}, and k_{RISC}) of these three emitters, the better performance of devices B and C could be rationalized by higher horizontal dipole ratios for PXZPyPM ($\Theta_{//}$ = 84%) and PXZTAZPM ($\Theta_{//}$ = 86%) relative to PXZPM ($\Theta_{//}$ = 73%). To further quantitatively analyze the contribution of the horizontal emitting dipole orientation on OLED device, we also conducted optical simulations on devices A to C according to the classical oscillating dipole equivalent model, optical parameters of the materials (fig. S1), and the measured $\Theta_{//}$s of three emitters. The simulated η_{out} of devices B and C were 39.1 and 39.7%, respectively, which are significantly higher than the reference device A (η_{out} = 34.0%). Because of the similar device architecture and the photoluminescence spectra, $\Theta_{//}$ is the only factor that can influence η_{out}. Therefore, the simulated results strongly indicate the beneficial influence of higher $\Theta_{//}$ on light extraction of OLEDs (Fig. 4F). To further clarify this point, we estimated the internal quantum efficiency (η_{int}) of our champion device B and the reference device A based on the following equation (*21*)

$$EQE = \eta_r \Phi_{PL} \gamma \eta_{out} = \eta_{int} \eta_{out}$$

where η_r refers to a fraction of radiative excitons, and γ represents the charge balance factor. The η_{int} of the PXZPyPM-based device B was calculated to be 0.867, the same as the PXZPM-based reference device A (η_{int} = 0.867). This clearly establishes that the superior EL performance of device B compared to the reference device A is solely due to the enhanced η_{out} of device B originating from the higher $\Theta_{//}$ of PXZPyPM over PXZPM. These findings manifest the tight connection between the emitting dipole orientation of TADF emitters, η_{out}, and electroluminescence efficiencies of the devices. Therefore, the selective modulation of emitting dipole orientation for TADF emitters via the acceptor plane expansion approach can substantially improve the corresponding performance of OLEDs.

DISCUSSION

In summary, the acceptor plane expansion approach allows us to construct green TADF emitters with preferentially horizontal emitting dipole orientation. With this strategy, two developed TADF emitters, PXZPyPM and PXZTAZPM, exhibited selectively strengthened horizontal emitting dipole orientation with only small influence on their excited states and the associated optoelectronic properties. PXZPyPM and PXZTAZPM preserved almost the same HOMO/LUMO

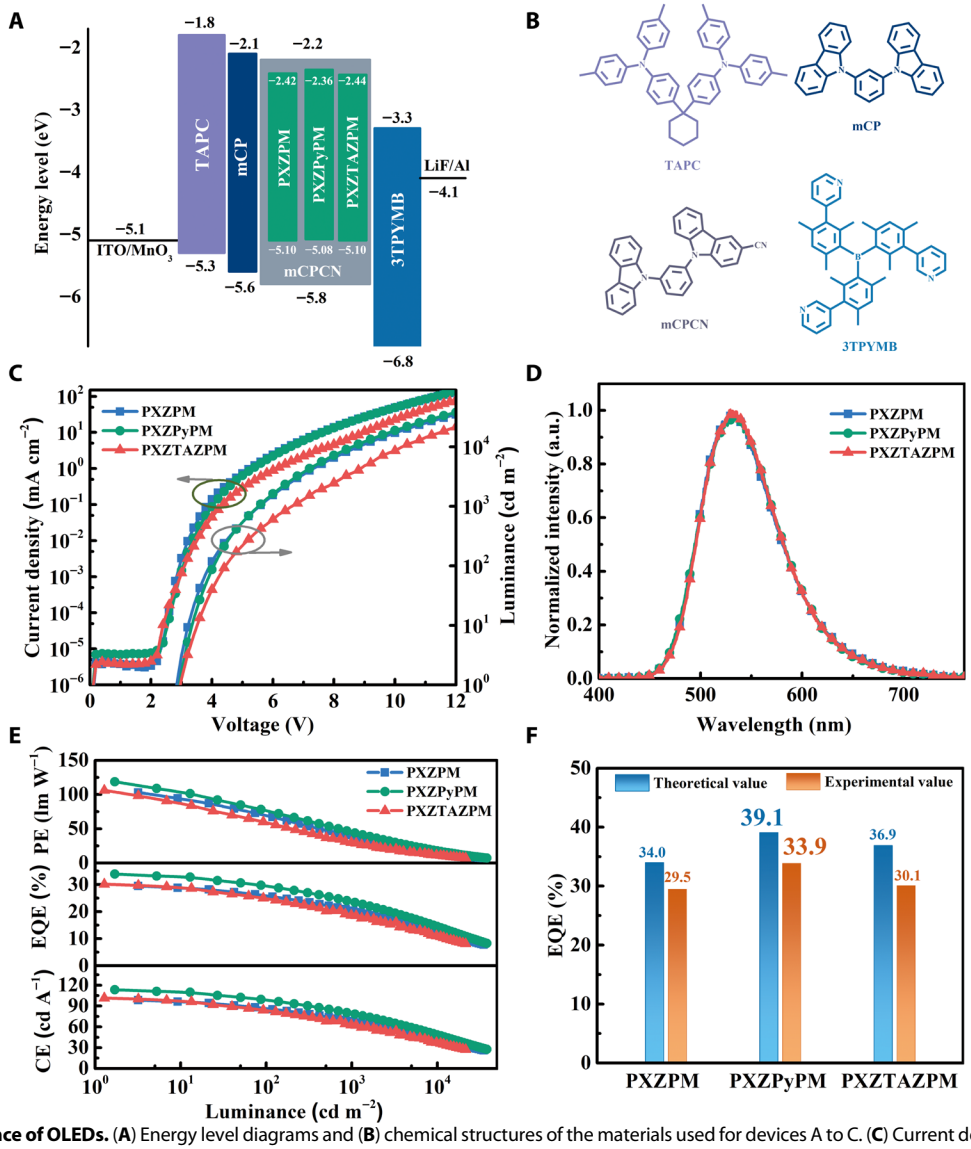

Fig. 4. Device performance of OLEDs. (**A**) Energy level diagrams and (**B**) chemical structures of the materials used for devices A to C. (**C**) Current density–voltage-luminance curves of devices A to C. (**D**) Electroluminescence spectra of devices A to C at 6 V. (**E**) PE, current efficiency (CE), and EQE versus luminance curves of devices A to C. (**F**) The comparison of theoretical EQEs and experimental EQEs.

Table 2. Electroluminescence characteristics of the devices.

Device	Emitter	V_{on}* (V)	Maximum efficiency†	Efficiency at 1000 cd m^{-2}‡	η_{out}§ (%)	$\eta_{out} \times \Phi_{PL}$‖ (%)	λ_{EL}¶ (nm)	CIE¶ (*x*, *y*)
			CE (cd A^{-1}), PE (lm W^{-1}), and EQE (%)	CE (cd A^{-1}), PE (lm W^{-1}), and EQE (%)				
A	PXZPM	3.0	98.4, 103.5, 29.5	68.5, 38.9, 20.5	34.0	34.0	528	(0.33, 0.58)
B	PXZPyPM	3.0	113.5, 118.9, 33.9	78.6, 44.6, 23.5	39.1	39.1	528	(0.33, 0.58)
C	PXZTAZPM	3.0	101.3, 106.1, 30.1	62.6, 29.5, 18.6	39.7	36.9	528	(0.33, 0.58)

*Turn-on voltage at 1 cd m^{-2}. †Maximum efficiencies of CE (cd A^{-1}), PE (lm W^{-1}), and EQE (%). The error for EQE is ±0.4%, which is obtained from five devices. ‡Electroluminescence efficiencies recorded at 1000 cd m^{-2}. §Calculated optical out-coupling efficiency. ‖Theoretical external quantum efficiencies. ¶Electroluminescence peaks and CIE 1931 coordinates recorded at 6 V.

energy levels and excited states and similar emission characteristics compared to the prototypical emitter of PXZPM. The expanded acceptor plane induced molecular orientation and emitting dipole orientation of both emitters to be horizontally aligned in the emitting layers. Consequently, the green OLED based on PXZPyPM achieved nearly 34% EQE and exceeding 118 lm W^{-1} PE, which are among the best results reported so far for green-to-yellow TADF OLEDs. This work could guide subsequent designs of TADF emitters with high horizontal ratios of emitting dipole orientation toward ultrahigh-efficiency TADF OLEDs.

MATERIALS AND METHODS

Synthesis and characterization

PXZPyPM and PXZTAZPM were synthesized according to literature precedence (*26*). PXZPyPM and PXZTAZPM were synthesized and characterized according to the methods described in fig. S2.

Theoretical calculation

DFT and TD-DFT simulations were performed using Gaussian 16 programs. Ground-state structures and frontier molecular orbitals were obtained by B3LYP density functional method with basis set 6-31G(d) (*29*). The isosurface threshold value was 0.02 for orbitals. TD-DFT with a non-empirically tuned range-separated functionals LC-BLYP with basis set 6-31G(d) were then performed to further analyze the excited states (*30*). S_1 and T_1 structures were both optimized with the polarizable continuum model, taking the dielectric constant for toluene (ε = 2.37) as a reference (*39*). Excited states analysis (including hole-electron distribution, overlap, oscillator strength, and other key parameters) was processed with the TD-DFT results using Multiwfn 3.6 program according to the program manual and literature method (*32*). The isosurface threshold value was 0.001 for hole and electron distributions of the excited states. Key parameters were listed in table S1. S_r describes the overlap of hole-electron distribution with the scale of [0, 1], as 0 means no overlap between hole-electron distribution, while 1 means perfect overlap between them.

The spatial range of the volume data was calculated according to the literature method (*35*). We quantified areas of the corresponding acceptor plane of three molecules using the isodensity surface at ρ = 0.001 e/bohr^3 generated by Marching Tetrahedra approach.

All atomistic molecular dynamics simulations were performed with the GROMACS 2019.1 software package (*40*). The bonded and nonbonded interaction parameters of mCPCN, PXZPM, PXZPyPM, and PXZTAZPM were built from the Generalized Amber Force Field parameter set (GAFF2) with the restrained electrostatic potential charges. Missing bonded parameters were generated by parmchk2 program. First, the force field parameters were validated by comparing the MM-optimized molecular geometries with the geometries obtained by DFT or MP2 methods and the x-ray crystallographic geometry. Subsequently, isothermal isobaric atomistic molecular dynamics simulations were performed on a 5 × 5 × 5 supercell for the mCPCN crystal. The supercell was equilibrated for 2.5 ns. In the simulations, a time step of 1 fs was set for the leapfrog integrator, and the temperature of 300 K and pressure of 1 atm were maintained by the Berendsen thermostat and barostat, respectively. A cutoff of 1.2 nm for the summation of van der Waals interaction and particle-mesh Ewald solver for long-range Coulomb interactions were used in the simulations. During the last 10 ns of the equilibrated trajectory, 1000 snapshots were sampled every 10 ps to analyze the geometric structures. In the atomistic molecular dynamics simulations, about 700 molecules (emitter/host mole ratio is 1:20, corresponding to ~6 wt % doping concentration of emitters) were deposited on the mCPCN (100) surface, and the resulting thickness of emitting layer film was about 10 nm. Six independent simulations were performed for each emitter/host system. Final statistical results were obtained as the average over these six trajectories.

Device fabrication and characterization of OLED performance

All organic materials used in experiments (except for the TADF emitters) were purchased from Lumtec Inc. OLEDs were fabricated on the ITO-coated glass substrates with multiple organic layers sandwiched between the transparent bottom ITO anode and the top metal cathode. All material layers were deposited by vacuum evaporation in a vacuum chamber with a base pressure of 10^{-6} torr. The current density-voltage-brightness (*J*-V-L) characterization of the light-emitting devices was performed with a source measurement unit and a spectroradiometer (DMS 201, AUTRONIC-MELCHERS GmbH). Electroluminescence spectra of devices were collected by a calibrated charge-coupled device spectrograph. The angular dependence of EL intensities (and spectra) was measured by a calibrated goniometric spectroradiometer (DMS 201, AUTRONIC-MELCHERS GmbH). The external quantum efficiencies of devices were determined by collecting the total emission fluxes with a calibrated integrating sphere measurement system and by measuring the angular distribution of the emission spectra and intensities.

SUPPLEMENTARY MATERIALS

Supplementary material for this article is available at http://advances.sciencemag.org/cgi/content/full/6/41/eaba7855/DC1

REFERENCES AND NOTES

1. T. D. Schmidt, T. Lampe, M. R. Daniel Sylvinson, P. I. Djurovich, M. E. Thompson, W. Brütting, Emitter orientation as a key parameter in organic light-emitting diodes. *Phys. Rev. Appl.* **8**, 037001 (2017).
2. J. Y. Kim, D. Yokoyama, C. Adachi, Horizontal orientation of disk-like hole transport molecules and their application for organic light-emitting diodes requiring a lower driving voltage. *J. Phys. Chem. C* **116**, 8699–8706 (2012).
3. M. Y. Wong, E. Zysman-Colman, Purely organic thermally activated delayed fluorescence materials for organic light-emitting diodes. *Adv. Mater.* **29**, 1605444 (2017).
4. H. Noda, H. Nakanotani, C. Adachi, Excited state engineering for efficient reverse intersystem crossing. *Sci. Adv.* **4**, eaao6910 (2018).
5. M. A. Baldo, D. F. O'Brien, Y. You, A. Shoustikov, S. Sibley, M. E. Thompson, S. R. Forrest, Highly efficient phosphorescent emission from organic electroluminescent devices. *Nature* **395**, 151–154 (1998).
6. P.-T. Chou, Y. Chi, Phosphorescent dyes for organic light-emitting diodes. *Chem. A Eur. J.* **13**, 380–395 (2007).
7. H. Uoyama, K. Goushi, K. Shizu, H. Nomura, C. Adachi, Highly efficient organic light-emitting diodes from delayed fluorescence. *Nature* **492**, 234–238 (2012).
8. Y. Liu, C. Li, Z. Ren, S. Yan, M. R. Bryce, All-organic thermally activated delayed fluorescence materials for organic light-emitting diodes. *Nat. Rev. Mater.* **3**, 18020 (2018).
9. M. J. Jurow, C. Mayr, T. D. Schmidt, T. Lampe, P. I. Djurovich, W. Brütting, M. E. Thompson, Understanding and predicting the orientation of heteroleptic phosphors in organic light-emitting materials. *Nat. Mater.* **15**, 85–91 (2016).
10. D. Yokoyama, H. Sasabe, Y. Furukawa, C. Adachi, J. Kido, Molecular stacking induced by intermolecular C-H···N hydrogen bonds leading to high carrier mobility in vacuum-deposited organic films. *Adv. Funct. Mater.* **21**, 1375–1382 (2011).
11. Y.-T. Lee, P.-C. Tseng, T. Komino, M. Mamada, R. J. Ortiz, M.-k. Leung, T.-L. Chiu, C.-F. Lin, J.-H. Lee, C. Adachi, C.-T. Chen, C.-T. Chen, Simple molecular-engineering approach for enhancing orientation and outcoupling efficiency of thermally activated delayed fluorescent emitters without red-shifting emission. *ACS Appl. Mater. Interfaces* **10**, 43842–43849 (2018).

12. Y. Watanabe, D. Yokoyama, T. Koganezawa, H. Katagiri, T. Ito, S. Ohisa, T. Chiba, H. Sasabe, J. Kido, Control of molecular orientation in organic semiconductor films using weak hydrogen bonds. *Adv. Mater.* **31**, 1808300 (2019).
13. M. Liu, R. Komatsu, X. Cai, K. Hotta, S. Sato, K. Liu, D. Chen, Y. Kato, H. Sasabe, S. Ohisa, Y. Suzuri, D. Yokoyama, S.-J. Su, J. Kido, Horizontally orientated sticklike emitters: Enhancement of intrinsic out-coupling factor and electroluminescence performance. *Chem. Mater.* **29**, 8630–8636 (2017).
14. T.-A. Lin, T. Chatterjee, W.-L. Tsai, W.-K. Lee, M.-J. Wu, M. Jiao, K.-C. Pan, C.-L. Yi, C.-L. Chung, K.-T. Wong, C.-C. Wu, Sky-blue organic light emitting diode with 37% external quantum efficiency using thermally activated delayed fluorescence from spiroacridine-triazine hybrid. *Adv. Mater.* **28**, 6976–6983 (2016).
15. T.-L. Wu, M.-J. Huang, C.-C. Lin, P.-Y. Huang, T.-Y. Chou, R.-W. Chen-Cheng, H.-W. Lin, R.-S. Liu, C.-H. Cheng, Diboron compound-based organic light-emitting diodes with high efficiency and reduced efficiency roll-off. *Nat. Photon.* **12**, 235–241 (2018).
16. Y.-L. Zhang, Q. Ran, Q. Wang, Y. Liu, C. Hänisch, S. Reineke, J. Fan, L.-S. Liao, High-efficiency red organic light-emitting diodes with external quantum efficiency close to 30% based on a novel thermally activated delayed fluorescence emitter. *Adv. Mater.* **31**, 1902368 (2019).
17. D. H. Ahn, S. W. Kim, H. Lee, I. J. Ko, D. Karthik, J. Y. Lee, J. H. Kwon, Highly efficient blue thermally activated delayed fluorescence emitters based on symmetrical and rigid oxygen-bridged boron acceptors. *Nat. Photon.* **13**, 540–546 (2019).
18. C. Mayr, S. Y. Lee, T. D. Schmidt, T. Yasuda, C. Adachi, W. Brütting, Efficiency enhancement of organic light-emitting diodes incorporating a highly oriented thermally activated delayed fluorescence emitter. *Adv. Funct. Mater.* **24**, 5232–5239 (2014).
19. P. Rajamalli, N. Senthilkumar, P.-Y. Huang, C.-C. Ren-Wu, H.-W. Lin, C.-H. Cheng, New molecular design concurrently providing superior pure blue, thermally activated delayed fluorescence and optical out-coupling efficiencies. *J. Am. Chem. Soc.* **139**, 10948–10951 (2017).
20. T. Komino, Y. Sagara, H. Tanaka, Y. Oki, N. Nakamura, H. Fujimoto, C. Adachi, Electroluminescence from completely horizontally oriented dye molecules. *Appl. Phys. Lett.* **108**, 241106 (2016).
21. K.-H. Kim, J.-J. Kim, Origin and control of orientation of phosphorescent and TADF dyes for high-efficiency OLEDs. *Adv. Mater.* **30**, 1705600 (2018).
22. K. Tuong Ly, R.-W. Chen-Cheng, H.-W. Lin, Y.-J. Shiau, S.-H. Liu, P.-T. Chou, C.-S. Tsao, Y.-C. Huang, Y. Chi, Near-infrared organic light-emitting diodes with very high external quantum efficiency and radiance. *Nat. Photon.* **11**, 63–68 (2017).
23. H. Shin, Y. H. Ha, H.-G. Kim, R. Kim, S.-K. Kwon, Y.-H. Kim, J.-J. Kim, Controlling horizontal dipole orientation and emission spectrum of Ir complexes by chemical design of ancillary ligands for efficient deep-blue organic light-emitting diodes. *Adv. Mater.* **31**, 1808102 (2019).
24. W. Zeng, S. Gong, C. Zhong, C. Yang, Prediction of oscillator strength and transition dipole moments with the nuclear ensemble approach for thermally activated delayed fluorescence emitters. *J. Phys. Chem. C* **123**, 10081–10086 (2019).
25. K. Wu, T. Zhang, L. Zhan, C. Zhong, S. Gong, N. Jiang, Z.-H. Lu, C. Yang, Optimizing optoelectronic properties of pyrimidine-based TADF emitters by changing the substituent for organic light-emitting diodes with external quantum efficiency close to 25% and slow efficiency roll-off. *Chem. A Eur. J.* **22**, 10860–10866 (2016).
26. Y. Xiang, Y. Zhao, N. Xu, S. Gong, F. Ni, K. Wu, J. Luo, G. Xie, Z.-H. Lu, C. Yang, Halogen-induced internal heavy-atom effect shortening the emissive lifetime and improving the fluorescence efficiency of thermally activated delayed fluorescence emitters. *J. Mater. Chem. C* **5**, 12204–12210 (2017).
27. K.-C. Pan, S.-W. Li, Y.-Y. Ho, Y.-J. Shiu, W.-L. Tsai, M. Jiao, W.-K. Lee, C.-C. Wu, C.-L. Chung, T. Chatterjee, Y.-S. Li, K.-T. Wong, H.-C. Hu, C.-C. Chen, M.-T. Lee, Efficient and tunable thermally activated delayed fluorescence emitters having orientation-adjustable CN-substituted pyridine and pyrimidine acceptor units. *Adv. Funct. Mater.* **26**, 7560–7571 (2016).
28. D. R. Lee, B. S. Kim, C. W. Lee, Y. Im, K. S. Yook, S.-H. Hwang, J. Y. Lee, Above 30% external quantum efficiency in green delayed fluorescent organic light-emitting diodes. *ACS Appl. Mater. Interfaces* **7**, 9625–9629 (2015).
29. A. D. Becke, Density-functional thermochemistry. III. The role of exact exchange. *J. Chem. Phys.* **98**, 5648–5652 (1993).
30. H. Iikura, T. Tsuneda, T. Yanai, K. Hirao, A long-range correction scheme for generalized-gradient-approximation exchange functionals. *J. Chem. Phys.* **115**, 3540–3544 (2001).
31. M. K. Etherington, J. Gibson, H. F. Higginbotham, T. J. Penfold, A. P. Monkman, Revealing the spin-vibronic coupling mechanism of thermally activated delayed fluorescence. *Nat. Commun.* **7**, 13680 (2016).
32. T. Lu, F. Chen, Multiwfn: A multifunctional wavefunction analyzer. *J. Comput. Chem.* **33**, 580–592 (2012).
33. N. J. Turro, V. Ramamurthy, J. C. Scaiano, *Modern Molecular Photochemistry* (University Science Books, USA, 2010).
34. W. Humphrey, A. Dalke, K. Schulten, VMD: Visual molecular dynamics. *J. Mol. Graph.* **14**, 33–38 (1996).
35. T. Lu, F. Chen, Quantitative analysis of molecular surface based on improved Marching Tetrahedra algorithm. *J. Mol. Graph. Model.* **38**, 314–323 (2012).
36. G. Hu, G. Han, Z. Tu, R. Duan, Y. Yi, Origin of high efficiencies for thermally activated delayed fluorescence organic light-emitting diodes: Atomistic insight into molecular orientation and torsional disorder. *J. Phys. Chem. C* **122**, 27191–27197 (2018).
37. P. Friederich, R. Coehoorn, W. Wenzel, Molecular origin of the anisotropic dye orientation in emissive layers of organic light emitting diodes. *Chem. Mater.* **29**, 9528–9535 (2017).
38. M.-S. Lin, S.-J. Yang, H.-W. Chang, Y.-H. Huang, Y.-T. Tsai, C.-C. Wu, S.-H. Chou, E. Mondal, K.-T. Wong, Incorporation of a CN group into mCP: A new bipolar host material for highly efficient blue and white electrophosphorescent devices. *J. Mater. Chem.* **22**, 16114–16120 (2012).
39. B. Mennucci, Polarizable continuum model. *WIREs Comput. Mol. Sci.* **2**, 386–404 (2012).
40. B. Hess, C. Kutzner, D. van der Spoel, E. Lindahl, GROMACS 4: Algorithms for highly efficient, load-balanced, and scalable molecular simulation. *J. Chem. Theory Comput.* **4**, 435–447 (2008).

Acknowledgments: We thank X. Cao and N. Li (Shenzhen University, P. R. China) for their assistance with the photoluminescence measurements. The numerical calculations in this paper have been performed on the supercomputing system in the Supercomputing Center of Wuhan University. **Funding:** S.G., C.Z., and C.Y. acknowledge financial support from the National Natural Science Foundation of China (51873158, 91833304, 51873160, and 51573141), the National Key R&D Program of China (2016YFB0401002), the Shenzhen Science and Technology Program (KQTD20170330110107046 and JCYJ20190808151209557), the Key Technological Innovation Program of Hubei Province (2018AAA013), and the Natural Science Foundation for Distinguished Young Scholars of Hubei Province (2017CFA033). C.-C.W. acknowledges the support from the Ministry of Science and Technology of Taiwan (MOST 108-2221-E-002-148-MY3 and 107-2221-E-002-160-MY3). W.-K.L. acknowledges the post-doctoral fellowship from Ministry of Education of Taiwan and Ministry of Science and Technology of Taiwan. **Author contributions:** S.G. and C.Y. conceived and designed the project. Y.X. synthesized the compounds and measured the photophysical, thermal, and electrochemical properties of the compounds. X.Y. synthesized one borate precursor. P.L., Y.-H.H., and C.-Y.W. fabricated the devices and analyzed the data. W.-K.L. performed the optical simulation of the devices. C.Z., W.Z., and Z.C. performed the quantum chemical calculations and molecular dynamics simulation. S.G., C.-C.W., and C.Y. supervised this research. All the authors discussed the results and contributed to the manuscript. **Competing interests:** The authors declare that they have no competing interests. **Data and materials availability:** All data needed to evaluate the conclusions in the paper are present in the paper and/or the Supplementary Materials. Additional data related to this paper may be requested from the authors.

Submitted 6 January 2020
Accepted 21 August 2020
Published 9 October 2020
10.1126/sciadv.aba7855

Citation: Y. Xiang, P. Li, S. Gong, Y.-H. Huang, C.-Y. Wang, C. Zhong, W. Zeng, Z. Chen, W.-K. Lee, X. Yin, C.-C. Wu, C. Yang, Acceptor plane expansion enhances horizontal orientation of thermally activated delayed fluorescence emitters. *Sci. Adv.* **6**, eaba7855 (2020).